Journal of Applied Mechanics and Technical Physics, Vol. 44, No. 4, pp. 506–515, 2003

GRAVITY WAVES DUE TO DISCONTINUITY DECAY OVER AN OPEN-CHANNEL BOTTOM DROP

V. I. Bukreev and A. V. Gusev

UDC 532.59

Experimental data are given on wave shapes and propagation speeds and characteristic headwater and tailwater depths after removal of a shield producing an initial free-surface level drop and located above a bottom drop in a rectangular open channel. Check is performed of self-similar solutions of the problem obtained earlier using a hydraulic approximation. It has been established that in certain ranges of time, longitudinal coordinate, and problem parameters, these solutions are supported by experimental results.

Key words: *liquid, free surface, discontinuous waves, experiment, verification of theory.*

Introduction. In hydraulics, the term "discontinuity decay" is used in solving the Cauchy problem with discontinuous piecewise constant initial data for the first approximation of shallow water theory [1]. In the present work, this term is used in a physical problem whose formulation is illustrated in Fig. 1. Decay of a liquid free-surface discontinuity in a channel with an even bottom has been studied to analyze hydrodynamic processes occurring upon a sudden dam break [2, 3]. Recently, discontinuity decay above a drop (sudden downstream drop in channel-bed level) or a step (sudden rise in channel-bed level) has been investigated in a number of computational and theoretical studies [4–6]. Solution of this problem is used to analyze accidents at ship locks [6]. Calculations and comparison with experiments for the case of discontinuity decay above an uneven bottom of a more complicated shape are performed in [7].

In the present paper, we report results of experimental studies of discontinuity decay above a drop and use them to verify the computational procedure of [6]. Experimental data on the height of overwash on a vertical wall can be found in [8, 9] for the case of discontinuity decay above an even bottom and in [10] for discontinuity decay above a drop.

In [6], theoretical self-similar solutions of the problem are considered within the framework of a hydraulic approximation. This approximation assumes that the pressure is distributed under a hydrostatic law. According to [6], a critical depth h_* is established above the drop:

$$h_0 = h_*, \qquad h_* = (q^2/g)^{1/3}, \qquad q = Q/B.$$

Here h_0 is the depth above the drop (Fig. 1), Q is the volumetric fluid discharge, and g is the acceleration of gravity. In this case, the critical depth is related to the initial depth above the drop H_1 by the formula $h_* = 4H_1/9$. The computational method of [6] is applicable only for $H_2 < H_2^*$ or $h_2 < H_2^*$ [$H_2^* = b + h_*$, h_2 is the height of the incident tailwater wave after removal of the shield, and b is the drop height (Fig. 1)]. Accounting for energy losses at the drop by introducing an empirical factor ζ is discussed in [6]. In the present paper, results of calculations using the method of [6] are given for the case of $\zeta = 0$.

Theory [6] yields four self-similar solutions for the free-surface profile: one for the headwater level depression wave and three for tailwater waves. In addition the theory allows one to calculate the flow depth h_3 (Fig. 1) and the wave propagation speed after reflection from the closed end of the channel.

Institute of Hydrodynamics, Siberian Division, Russian Academy of Sciences, Novosibirsk 630090. Translated from Prikladnaya Mekhanika i Tekhnicheskaya Fizika, Vol. 44, No. 4, pp. 64–75, July–August, 2003. Original article submitted December 10, 2002.

 0021-8944/03/4404-0506 $25.00

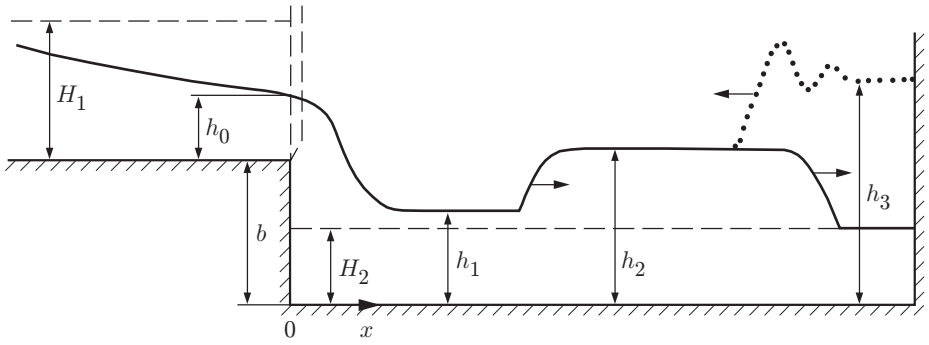

Fig. 1. Diagram of the experiment.

Experimental Technique. A diagram of the experiment with the basic designations is shown in Fig. 1. The experiments were performed in a rectangular channel of width $B = 20.2$ cm. A drop of height $b = 7.2$ cm was placed at $l = 1.93$ m from the right closed end of the channel. The left open end of the channel was attached to a tank 3.3 m long and 1 m wide located at $l_1 = 2.27$ m from the drop. This setup simulated conditions typical of a ship lock ahead of which there is an outer harbor with a large free-surface area. The initial headwater depth H_1 was specified by means of an even shield located above the drop (Fig. 1). The cases of $H_2 \neq 0$ ("wet bottom") and $H_2 = 0$ ("dry bottom") are considered depending on the initial tailwater depth H_2 [3]. Next, wave propagation over a "wet bottom is analyzed." The parameters b, l, and l_1 were unchanged in the experiment. The initial free-surface levels were determined by measuring needles with an absolute error not larger than 0.05 cm. Headwater depths were measured from the channel bottom ahead of the drop, and tailwater depths were measured from the bottom behind the drop.

At the time $t_0 = 0$, the shield was manually removed from the channel. The law of its motion was recorded by a slide-wire gauge. The time of removal of the shield did not exceed 0.05 sec with the smallest time of wave propagation from the drop to the closed end of the channel equal to 1.3 sec. Fluctuations in the free-surface level as a function of time t at given points on the longitudinal coordinate x were measured by wavemeters operating by the principle of a difference in electric conductivity between water and air. The resolving power of the wavemeters was 0.2 mm. The upper bound of the fluctuation frequency traced by the wavemeters with an error not larger than 10% was 10 Hz. Photo and video recording were also employed. In the further consideration, we focus on time periods over which the wave reflected from the free end did not reach the channel cross section on the plots presented below.

Experimental Results and Comparison with Theory. Figure 2 gives experimental and calculation data for the headwater depression wave after removal of the shield (here and below, the standard error of the characteristic depths did not exceed the size of experimental points). The figure also shows the time variation ($\tau = t\sqrt{g/H_1}$) of the flow depth h_0/H_1 directly above the drop ($x = 0$) and the depth $h(x,t)/H_1$ at two headwater points ($x < 0$). Time is reckoned from the moment of removal of the shield. Horizontal dashed curves show two characteristic depths. Line 4 corresponds to the depth h_*. In some problems of hydraulics, it is useful to introduce the concept of the second critical depth $h_{**} = 0.77h_*$ [11]. In Fig. 2, this depth is shown by horizontal dashed line 5. The physical sense of the second critical depth is discussed in [11], where, in particular, it is shown experimentally that for a steady flow in a channel with an equal horizontal bottom, exactly this depth takes place at the entrance from the channel to the atmosphere.

According to theory [6], a constant depth equal to h_* is established instantaneously above a drop. In an infinitely long channel, $h \to h_*$ as $t \to \infty$ for all $x < 0$. In the experiment, a constant depth above the drop was not established instantaneously (experimental points 1 in Fig. 2) and in a certain time interval it coincided with h_{**} rather than with h_*. Thus, in the unsteady problem of discontinuity decay above a drop there are time intervals and parameter ranges in which the second critical depth is established above the drop. The vertical dashed curves in Fig. 2 correspond to five characteristic times. According to [6], a depression wave propagates at speed $c_0 = \sqrt{gH_1}$, and at times τ_1 and τ_2, it should reach the wavemeters located at two distances upstream of the drop. In the experiment, the time during which the perturbation reached the wavemeters was smaller than that in the calculations considered. Additional analysis shows that for the experimental conditions corresponding to Fig. 2, the leading perturbation edge propagated at the second critical speed $c_{**} = 1.3c_0$. The physical sense of the second critical speed and its manifestation in other nonlinear unsteady processes is discussed in [12].

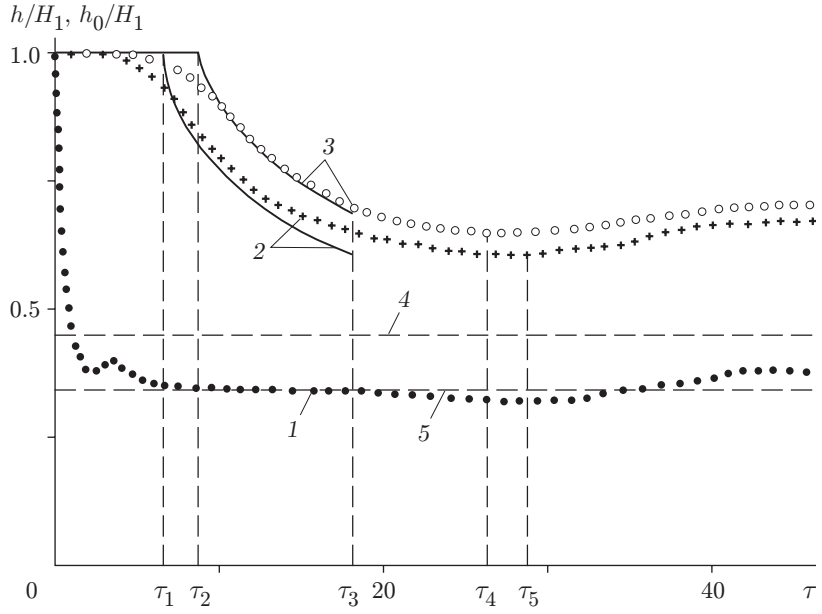

Fig. 2. Time variation of the flow depth above the drop at $H_1/b = 1.74$ and $H_2/b = 0.78$: 1 refer to h_0/H_1, 2 and 3 refer to h/H_1 for $x/H_1 = 6.4$ (2) and 8.8 (3), 4 refer to h_*/H_1, and 5 refer to h_{**}/H_1; solid curves refer to calculations and points refer to the experiment.

At the time τ_3, the depression wave reached the open end of the channel. Beginning from this time, comparison with theory becomes incorrect because of a difference in boundary conditions. In [6], a channel of infinite length is considered. In the experiment, a sudden widening of the channel occurred at $x = -l_1$, and a constant free-surface level was established at $\tau > \tau_3$. At the times τ_4 and τ_5, the wave reflected from free end of the channel reached the wavemeters, which was accompanied by a slow rise in the free-surface level.

From Fig. 2, it follows that at a relatively small distance upstream of the drop, the self-similar solution [6] for the depression wave agrees well with the experiment. However, at large distances, there is a difference due to the fact that the experimental speed of perturbation propagation is higher than calculated values (experimental points and curve 2 in Fig. 2).

Fuller information on the depth h_0 directly above the drop in time intervals where its value was constant is presented in Figs. 3 and 4. Figure 3 gives a curve of h_0/b versus H_2/b for a constant value of H_1/b. The adopted value of H_1/b corresponds to the characteristic headwater depth at the ship lock of the Novosibirsk hydroelectric power station at a scale of 1 : 100. The depths H_1/b and h_0/b were measured from the channel bottom ahead of the drop, and the depth H_2/b was measured from the channel bottom behind the drop. The horizontal dashed line 1 corresponds to the limiting value of $h_0/b = H_1/b$; line 2, to the critical depth h_*/b; line 3, to the second critical depth $h_{**}/b \approx 0.77h_*/b$; and the vertical dashed line 5, to the value of $H_2/b = 1 + h_*/b$. In [6], it is assumed that this equality corresponds to transition from the nonsubmerged state of head and tail conjugation to the submerged state. By the definition of [13], the state of head and tail conjugation is called nonsubmerged if the tailwater processes do not influence the headwater flow; otherwise, the state of conjugation is submerged. For the submerged state (to the right of line 5), the theory of [6] is inapplicable.

In the experiment, at a tailwater depth smaller than the drop height, the second critical depth was established directly above the drop. The first critical depth above the drop took place for the single value $H_2/b = 1 + 0.51h_*/b$, which corresponds to the vertical dashed line 4 in Fig. 3. Thus, transition from the nonsubmerged to the submerged state of head and tail conjugation due to discontinuity decay above the drop occurs at a smaller tailwater depth than that in steady flow a behind a wide sill.

Figure 4 shows a curve of h_0/b versus H_1/b for a constant value of $H_2/b < 1$. The adopted value of H_2/b corresponds to the characteristic tailwater depth at the ship lock of the Novosibirsk hydroelectric power station at a scale of 1 : 100. The dashed curve 1 shows the theoretical relation $h_0 = h_* = 4H_1/9$. The solid curve 2 corresponds to the second critical depth. In this series of experiments, the constant depth above the drop also coincided with the second critical depth.

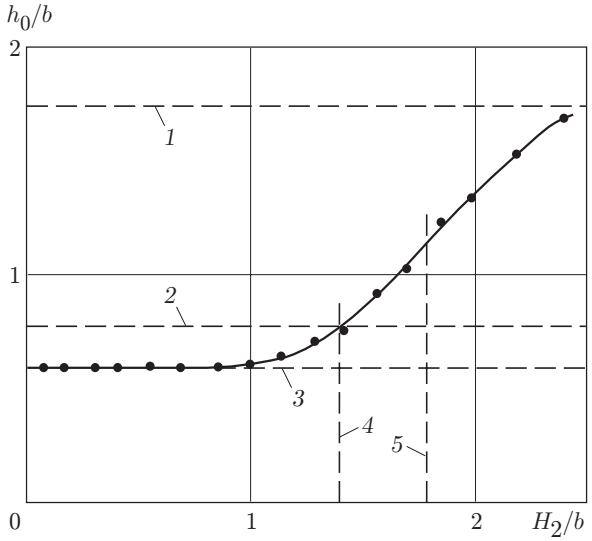

Fig. 3

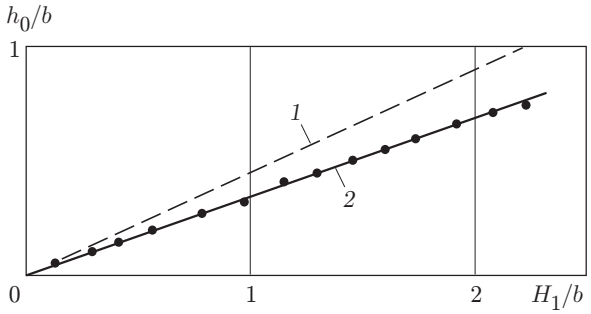

Fig. 4

Fig. 3. Depth above the drop at $H_1/b = 1.74$: 1 refres to $h_0/b = H_1/b$, 2 to $h_0 = h_*$, 3 to $h_0 = h_{**}$; lines 4 and 5 show the upper boundary of the nonsubmerged regime (4 refers to the experiment and 5, to calculations).

Fig. 4. Depth above the drop at $H_2/b = 0.69$: curve 1 refers to $h_0 = h_*$ and curve 2 to $h_0 = h_{**}$.

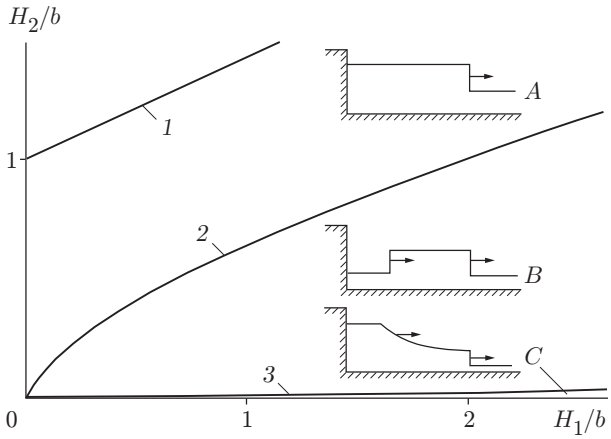

Fig. 5. Theoretical self-similar tailwater wave profiles: 1 refers to $H_2 = H_2^*$; 2 is the boundary separating the existence regions of the profiles A and B and 3 is the boundary separating the existence regions of the profiles B and C.

It should be noted that in the experiment, the critical depth h_* also was established but this occurred at a rather small distance upstream and not directly above the drop. Therefore, the difference between the experimental and calculated depths directly above the drop does not lead to a considerable difference in the shapes and parameters of the tailwater waves considered below.

Self-similar tailwater free-surface profiles are given in Fig. 5. Curve 1 is the upper boundary of the region of applicability of theory according to the condition $H_2 < H_2^*$. Curves 2 and 3 correspond to the theoretical boundaries of the existence region of various self-similar wave patterns on the "phase plane" of the parameters $(H_1/b, H_2/b)$ for $b = 7.2$ cm.

On the profile A there is one discontinuous wave propagating downstream at speed D. In real situations, the discontinuous wave corresponds to a hydraulic jump. There are several shapes of hydraulic jumps, of which the main types are a jump with a head roller and a smooth undular jump [13]. The term "bore" is used for a moving

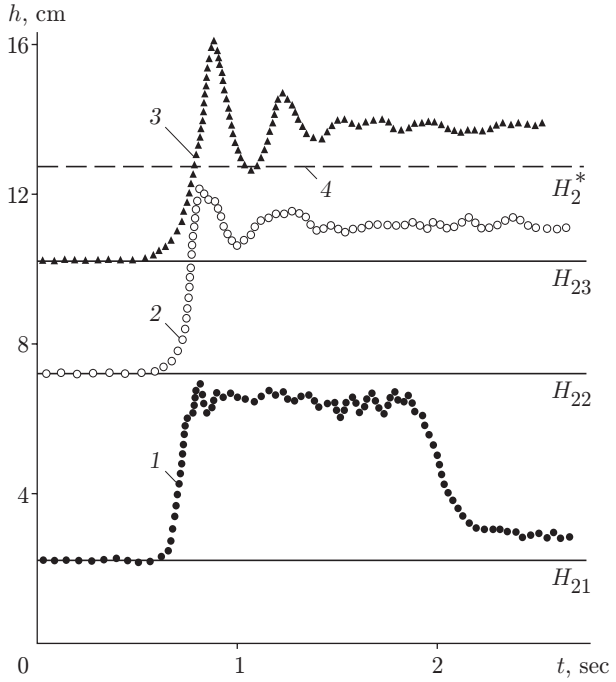

Fig. 6. Time variation of the free-surface level at $H_1/b = 1.74$ and $x/b = 15.3$: 1) $H_2/b = H_{21}/b = 0.31$; 2) $H_2/b = H_{22}/b = 1.0$; 3) $H_2/b = H_{23}/b = 1.42$; 4) theoretical upper boundary of the nonsubmerged state.

hydraulic jump. In theory [6], all bore shapes are described by a free-surface level discontinuity. The profile B in Fig. 5 is characterized by the existence of two discontinuous wave propagating downstream (the trailing wave moves more slowly than the leading wave). On the profile C, the trailing discontinuous wave was transformed into a smooth depression wave propagating downstream.

Experimental determination of the boundaries separating self-similar profiles is an independent labor-consuming problem beyond the scope of the present work. It is complicated by the fact that in experiments, it is difficult to formulate criteria for determining these boundaries because in their neighborhood there are several transitional shapes of waves. Experiments only showed that one bore (profile A) formed above the theoretical boundary 2 and two bores (profile B) formed between boundaries 2 and 3. As regards C-type waves, they are nearly unfeasible. Even for the conditions of the Novosibirsk ship lock, the theoretical existence region of this wave corresponds to a tailwater depth less than 12 cm [6]. In laboratory experiments, this depth should be less than 1.2 mm. In this case, of significance is the effect of small variations of geometrical parameters, in particular, the roughness of the channel bottom and walls.

Figure 6 gives typical examples of the experimental tailwater wave recorded by fixed wavemeters. The wavemeter gives information on the fluctuations in the free-surface level in time and does not distinguish the wave propagation direction. In the wavemeter signal, the leading wave edge is located on the left. The tailwater waves propagated to the right (see Fig. 1). In this series of experiments, only the tailwater depth was varied.

The depth H_{21} corresponds to the existence region of two jumps (curve 1 in Fig. 6), which was confirmed by experimental data. The depth H_{22} corresponds to the existence region of one jump. This was also confirmed qualitatively in experiments, but the experimental bore (curve 2) has undulations along with a head roller. For the initial depth H_{23}, the theory is inapplicable according to the condition $h_2 < H_2^*$. In the experiments, there was also one wave (curve 3) at this depth but it had the shape of a smooth undular bore rather than a classical bore with a head roller.

Of greatest interest is the self-similar solution for a B-type wave with two discontinuities (see Fig. 5). Figure 7 gives a frame of the wave corresponding to this solution. The vertical scale is 1.43 times larger than the horizontal one. The hydraulic jumps move to the right. Directly behind the drop, one can see an air cavity that existed for parameter values $H_2 < 0.9b$ and $H_1 > 4\sqrt{\sigma/(\rho g)}$ (σ is the surface tension and ρ is the water density) during the

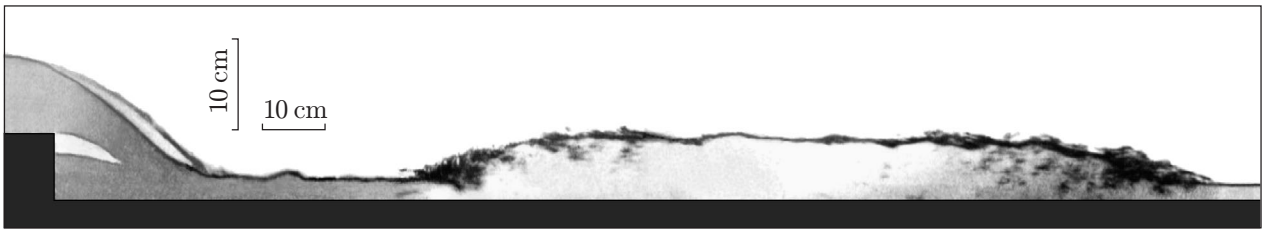

Fig. 7. Experimental B-type waves at $H_1 = 12.5$ cm, $H_2 = 2.2$ cm, and $t \approx 1.03$ sec.

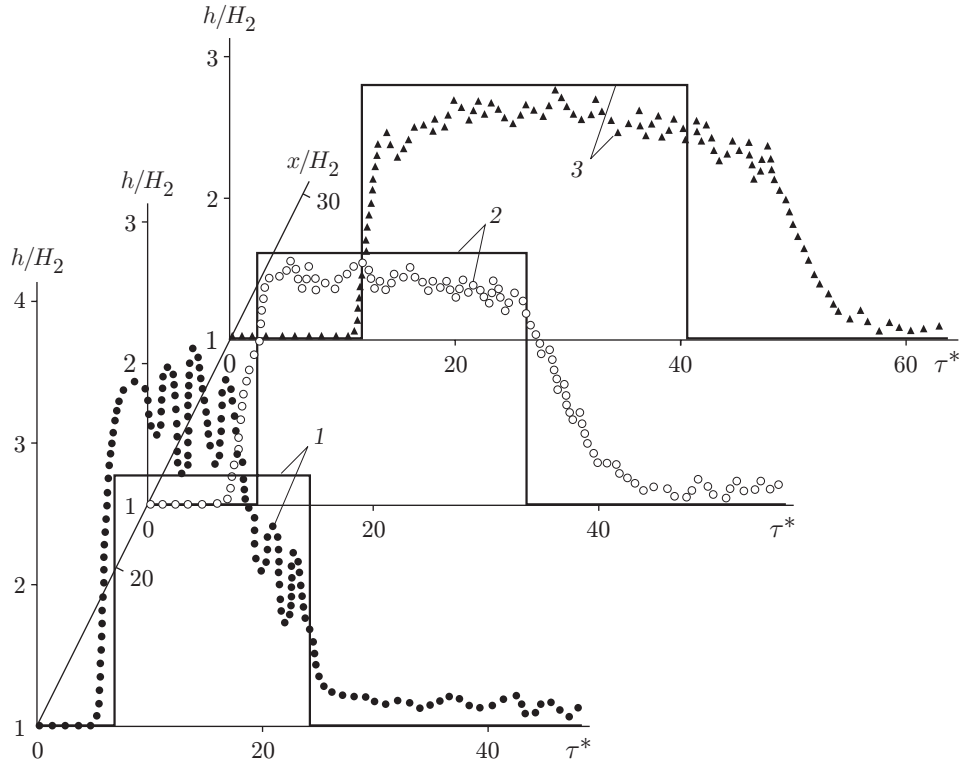

Fig. 8. Comparison of calculated (solid curves) and experimental (points) data for a B-type wave at $H_1/b = 2.08$, $H_2/b = 0.44$ and $x/H_2 = 15.6$ (1), 21.9 (2), and 26.7 (3).

entire time interval from the moment of removal of the shield to the time of arrival of the wave reflected from the closed end of the channel. Fuller information on cavities in steady flows behind a sill is contained in [14].

Results of experimental verification of the self-similar solution for B-type waves are given in Fig. 8. The calculations results are presented as curves of h/H_2 versus the time $\tau^* = t\sqrt{g/H_2}$ (solid curves). The points show the corresponding experimental data. The time is reckoned from the moment of removal of the shield. The depths were measured from the channel bottom behind the drop. It is evident that at $x/H_2 = 21.9$, the calculated and experimental data agree fairly well. At $x/H_2 = 15.6$, the flow has not yet entered a self-similar regime. At $x/H_2 = 26.7$, there is a deviation of the experimental wave shape from the self-similar solution, which shows up primarily as a decrease in the speed of propagation of the trailing edge.

Figure 9 shows a curve of the depth behind the leading edge of the wave h_2 versus the initial tailwater depth H_2 for a constant headwater depth $H_1 = 12.5$ cm. The solid curve 1 refers to a calculation using the theory of [6]. This theory is applicable only to the left of the vertical dashed curve 5 [6]. The vertical dashed curve 4 separates the existence regions of A-type waves with one hydraulic jump (to the right of the curve 4) and B-type waves with two hydraulic jumps. Curves 2 and 3 in Fig. 9 approximate experimental data. In the experiment with rather large values of H_2, there were undulations behind the leading edge of the wave (see Fig. 6). At a certain distance behind the leading edge, the undulations damped and a constant value $h_2 = h_2^{as}$ (curve 2) was established. For curve 3, $h_2 = h_2^{\max}$ ($h_2^{\max}$ is the maximum depth corresponding to the first crest of the undular hydraulic jump).

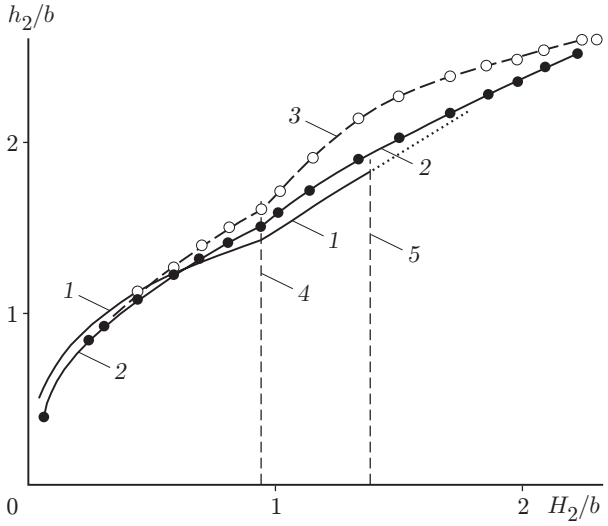

Fig. 9

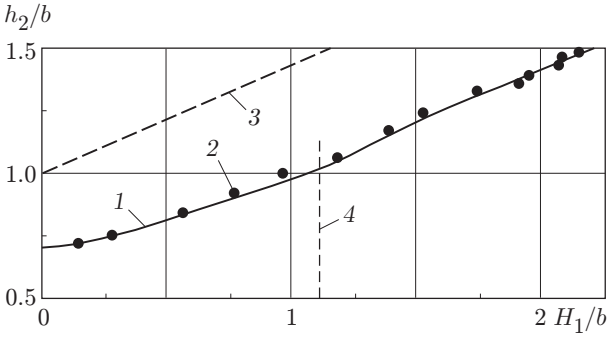

Fig. 10

Fig. 9. Depth behind the leading edge of a tailwater wave at $H_1/b = 1.74$: curve 1 and points 2 refer to calculated and experimental values of h_2^{as}, respectively, and curve 3 refers to experimental values of $h_2^{\max}$; 4 is the boundary separating the self-similar solutions for A and B-type waves and 5 is the experimental upper boundary of the nonsubmerged state.

Fig. 10. Depth behind the leading edge of the wave at $H_2/b = 0.69$: curve 1 and points 2 refer to calculated and experimental data, respectively; 3 is the upper boundary of the region of applicability of the theory by the condition $H_2 < b + 4H_1/9$ and 4 is the boundary of the existence region of A-type waves (to the left of the curve) and B-type waves.

For the indicated value of H_1, the depth $h_2^{\min}$ corresponding to the first trough of the undular jump nearly coincided with h_2.

Figure 10 shows a curve of h_2 versus H_1 at $H_2 = 5$ cm. Curve 1 refers to calculated values of h_2. The experimental points 2 correspond to values of h_2^{as}. For the indicated value of H_2, the undulations were insignificant, and the values of $h_2^{\max}$ and $h_2^{\min}$ almost coincided with h_2^{as}. The dashed curve 3 in Fig. 10 is the upper boundary of the region of applicability of the theory of [6]. The data in Figs. 9 and 10 demonstrate that the experimental values of h_2^{as} agree well with calculated values of h_2.

Of great importance for analysis of accidents at ship locks is information on the rise in the water level on the butt-end wall h_3 upon reflection of the waves considered in the present work. In [6], the value of h_3 is constant over the time interval from the moment of beginning of reflection to the moment of arrival of the waves that reflected from the drop for the second time. In the experiment, a vertical jet rising at a great height first forms on the wall. If the energy of the incident wave is sufficiently high, the jet breaks up into drops. Experimental data for this stage of reflection of the waves considered are given in [10]. At the next stage, an undular bore (smooth or having a breaking leading edge) detaches from the wall. On the wall, one observes damped fluctuations in the depths with a maximum value $h_3^{\max}$ (for the first crest of the undular bore) and a minimum value $h_3^{\min}$ (for the first through of the undular bore). These fluctuations decrease with time and a constant depth h_3^{as} is then established. Calculated values of the depth h_3 and experimental values of the depths $h_3^{\max}$, $h_3^{\min}$, and h_3^{as} are given in Figs. 11 and 12. The data in Fig. 11 are obtained for a constant value $H_1 = 12.5$ cm, and those in Fig. 12, for a constant value $H_2 = 5$ cm. The wavemeter was placed at 2 cm ahead of the right butt-end wall of the channel. Figure 13 shows a correlation of the calculated h_3 and experimental h_3^{as} depths near the butt-end wall of the channel for various combinations of parameters in the ranges $0.14 \leqslant H_1/b \leqslant 2.22$ and $0.4 \leqslant H_2/b \leqslant 1.5$. For an ideal correlation, the points in Fig. 13 should be located on the bisector of the coordinate angle shown by a solid curve.

From the data given in Figs. 11–13, it follows that the calculated values of h_3 agree well with the experimental data for h_3^{as}. However, at some times in the experiment, there was a much greater rise in the free-surface level both on the wall and at other points on the longitudinal coordinate because of undulations. It should be noted that the theory of [6] is valid only for the nonsubmerged state of head and tail conjugation behind the drop; therefore, the discrepancy between the calculated and experimental data to the right of curve 5 in Fig. 11 is quite reasonable.

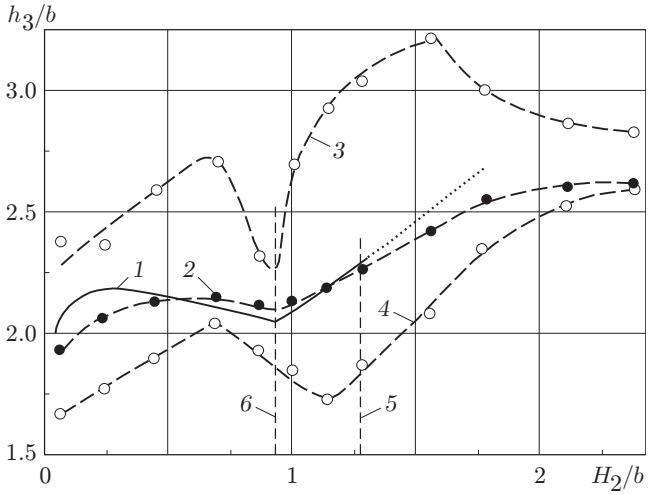

Fig. 11. Depth near the closed end of the channel at $H_1/b = 1.74$: curve 1 and points 2 refer to calculated and experimental values of h_3^{as}, respectively, and points 3 and 4 refer to experimental values of $h_3^{\max}$ and $h_3^{\min}$, respectively; 5 is the experimental upper boundary of the nonsubmerged state mode; 6 is the boundary separating the self-similar solutions for A and B-type waves.

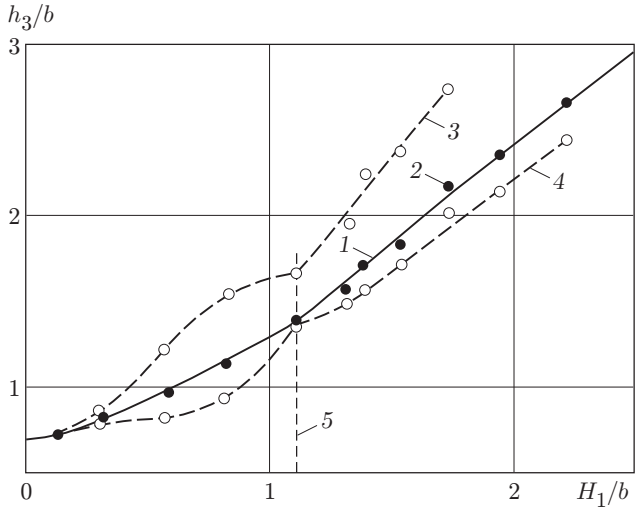

Fig. 12. Depth near the closed end of the channel at $H_2/b = 0.69$: curve 1 and points 2 refer to calculated and experimental values of h_3^{as} and points 3 and 4 refer to experimental values of $h_3^{\max}$ and $h_3^{\min}$, respectively; 5 is the boundary separating the self-similar solutions for A and B-type wave.

Calculated and experimental data on the propagation speed D of the leading edge of a wave (in a fixed coordinate system) before its reflection from the vertical wall at $H_1 = 12.5$ cm ahead of the drop are given in Fig. 14, and those at $H_2 = 5$ cm behind the drop are given in Fig. 15 (the measurement error D is shown by vertical line segments). We note that in experiment, difficulties arise in measuring the propagation speed of the waves considered here. First of all, a rigorous definition of the propagation speed can be given only for fixed waves whose shape is unchanged in a coordinate system moving with the wave or for the self-similar solutions obtained in [6]. In experiments, the stationarity or self-similarity conditions, strictly speaking, are not satisfied because of energy dissipation. Another complicating factor is the existence of an unstable roller at the leading edge of a classical hydraulic jump.

In the experiment, the speed of propagation of a specified point on the wave profile is adopted as an equivalent of the theoretical propagation speed. The experimental data in Figs. 14 and 15 are obtained for the point at half-height of the leading edge of the wave by measuring the travel time Δt of this point in a specified interval of the longitudinal coordinate Δx between two fixed wavemeters. Of significance is the coordinate x of the middle of the interval Δx by which the measured values of $D = \Delta x/\Delta t$ are normalized. In the experiments, the values of x

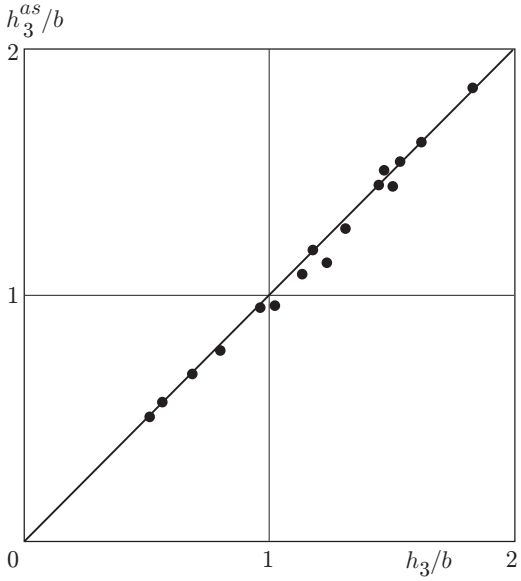

Fig. 13

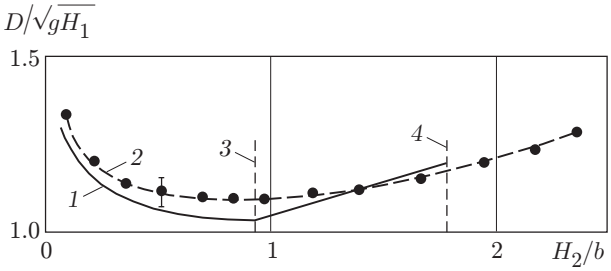

Fig. 14

Fig. 13. Correlation of calculated and experimental depths near the closed end of the channel.

Fig. 14. Propagation speed of the leading edge of the bore at $H_1/b = 1.74$: curve 1 and points 2 refer to calculated and experimental data, respectively; 3 is the boundary separating the self-similar solutions for A and B-type waves and 4 is the boundary of the region of applicability of the theory by the condition $H_2 < b + 4H_1/9$.

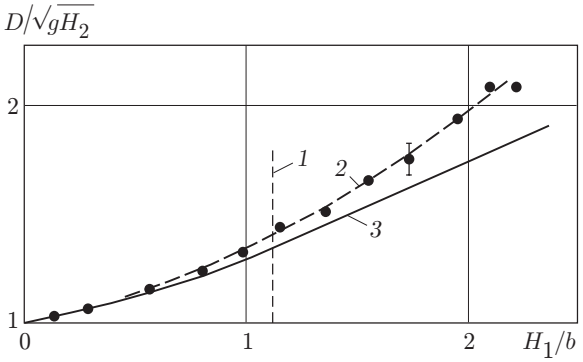

Fig. 15. Propagation speed of the leading edge of the bore at $H_2/b = 0.69$: 1 is the boundary separating the self-similar solutions for A and B-type wave; points 2 and curve 3 refer to the experimental and calculated data, respectively.

(downstream of the drop) were chosen such that the depth h_2^{as} was constant. The values of Δx were varied from 20 to 100 cm with other things being equal. The difference of the measurement results was within the random error due to instability of the hydraulic jump roller. To decrease the random error for some combinations of parameters, experiments were repeated three or four times, and their results were averaged. Nevertheless, the experimental error of D was greater than the error in determining the characteristic depths.

In view of the aforesaid, the agreement between the calculated and experimental data in Figs. 14 and 15 is satisfactory. The largest difference (14%) took place in the series of experiments with $H_2/b = 0.69$ at $H_1/b = 2.1$ (see Fig. 15). Observation showed that for this combination of parameters, the wave head had a shape intermediate between a classical hydraulic jump (for smaller values of H_2) and a smooth undular jump (for large values of H_2).

Conclusions. The theoretical self-similar wave shapes due to discontinuity decay over a drop [6] occur in the nonsubmerged state of head and tail conjugation in experiments. The theoretical values of the propagation speeds and average heights of waves under conditions of accidental break of ship lock gates also agree satisfactorily with experimental values. At the same time, the self-similar solutions have a limited region of applicability on the longitudinal coordinate, in time, and in the space of parameters. The degeneration of the self-similar wave shapes is basically related to energy losses. The model of [6] takes into account only part of energy losses directly behind the sill by introducing a factor ζ that depends on problem parameters. However, the value of this factor is unknown, and in the calculations, it was assumed to be $\zeta = 0$. If one sets $\zeta \neq 0$, the boundaries between different self-similar solutions, wave heights, and propagation speed will change but the wave shape will not change.

In real situations, energy loss also occurs during wave propagation. In particular, in the case of B-type waves, the fluid behind its trailing edge moves at a high speed in a supercritical regime, which is accompanied by considerable energy losses due to friction. As a result, in a channel with a zero bottom slope, the depth behind the wave h_1 increases continuously on the coordinate x and its conjugate depth h_2 decreases.

With time, the classical bore becomes an undular bore first at the trailing edge and then at the leading edge of the B-type wave. The undular bore breaks up into solitary waves. In the further process, the waves become linear because of energy dissipation. The mathematical model of [15], taking into account wave dispersion and mixing upon breaking and energy loss, holds promise for describing the degeneration of a classical hydraulic jump.

We thank A. A. Atavin for useful discussions and E. M. Romanov for assistance in the experiment.

This work was supported by the Russian Foundation for Fundamental Research (Grant No. 01-01-00846) and the Federal purpose-oriented program "Integration of Science and Higher Education in Russia" (Grant No. I0931).

REFERENCES

1. A. A. Atavin, M. T. Gladyshev, and S. M. Shugrin, "Discontinuous flows in open channels," in: *Dynamics of Continuous Media* (collected scientific papers) [in Russian], No. 22, Novosibirsk (1975), pp. 37–64.
2. R. F. Dressler, "Comparison of theories and experiments for the hydraulic dam-break wave," *Int. Assoc. Sci. Hydrology*, **3**, No. 38, 319–328 (1954).
3. J. J. Stoker, *Water Waves. The Mathematical Theory with Applications*, Interscience Publ., New York–London (1957).
4. F. Alcrudo and F. Benkhaldon, "Exact solutions to the Riemann problem of shallow water equations with bottom step," *Comput. Fluids*, **30**, 643–671 (2001).
5. V. V. Ostapenko, "Discontinuous solutions of the shallow water equations for flow over a bottom step," *J. Appl. Mech. Tech. Phys.*, **43**, No. 6, 836–874 (2002).
6. A. A. Atavin and O. F. Vasil'ev, "Possible consequences of accidents at ship locks due to penstock failure," in: *Hydraulic and Hydrological Aspects of Reliability and Safety Assessment of Hydraulic Structures*, Abstracts of Int. Symp. (St. Petersburg, May 28–June 1, 2002), Inst. of Hydraulic Engineering, St. Petersburg (2002), p. 121.
7. V. A. Prokof'ev, "Modern numerical schemes based on the control volume method for simulating rapid flows and dam-break waves," *Gidrotekh. Stroit.*, **7**, 22–29 (2002).
8. V. I. Bukreev and A. V. Gusev, "Reflection of a dam-break wave from a vertical wall," in: *Trans. Novosib. State Architectural University*, Vol. 3, No. 2 (2000), pp. 47–59.
9. V. B. Barakhnin, T. V. Krasnoshchekova, and I. N. Potapov, "Reflection of a dam-break wave at a vertical wall. Numerical modeling and experiment," *J. Appl. Mech. Tech. Phys.*, **42**, No. 2, 269–276 (2001).
10. V. I. Bukreev, "Water impingement on a vertical wall due to discontinuity decay above a drop," *J. Appl. Mech. Tech. Phys.*, **44**, No. 1, 59–63 (2003).
11. V. I. Bukreev and A. V. Gusev, "Waves behind a step in an open channel," *J. Appl. Mech. Tech. Phys.*, **44**, No. 1, 52–58 (2003).
12. V. I. Bukreev and A. V. Gusev, "Waves in a channel ahead of a vertical plate," *Izv. Ross. Akad. Nauk, Mekh. Zhidk. Gaza*, **1**, 82–90 (1999).
13. P. G. Kiselev, *Handbook on Hydraulic Calculations* [in Russian], Gosénergoizdat (1957).
14. V. I. Bukreev and A. V. Gusev, "Cavities behind a spillway with a wide sill," *J. Appl. Mech. Tech. Phys.*, **43**, No. 2, 280–285 (2002).
15. V. Yu. Liapidevskii and V. M. Teshukov, *Mathematical Models of Long-Wave Propagation in Inhomogeneous Liquids* [in Russian], Izd. Sib. Otdel. Ross. Akad. Nauk, Novosibirsk (2000).